

## Article

# Activated Carbon for CO<sub>2</sub> Adsorption from Avocado Seeds Activated with NaOH: The Significance of the Production Method

Joanna Siemak<sup>1</sup>, Grzegorz Mikołajczak<sup>2</sup>, Magdalena Pol-Szyszko<sup>3</sup> and Beata Michalkiewicz<sup>1,\*</sup> 

<sup>1</sup> Department of Catalytic and Sorbent Materials Engineering, Faculty of Chemical Technology and Engineering, West Pomeranian University of Technology in Szczecin, Piastów Ave. 42, 71-065 Szczecin, Poland; joanna.siemak@zut.edu.pl

<sup>2</sup> Faculty of Electrical Engineering, West Pomeranian University of Technology in Szczecin, 26 Kwietnia St. 10, 71-126 Szczecin, Poland; grzegorz.mikolajczak@zut.edu.pl

<sup>3</sup> Department of Plant Genetics, Breeding and Biotechnology, Faculty of Environmental Management and Agriculture, West Pomeranian University of Technology in Szczecin, 17 Słowackiego Str., 71-434 Szczecin, Poland; magdalena.pol-szyszko@zut.edu.pl

\* Correspondence: beata.michalkiewicz@zut.edu.pl

**Abstract:** The rise in atmospheric greenhouse gases like CO<sub>2</sub> is a primary driver of global warming. Human actions are the primary factor behind the surge in CO<sub>2</sub> levels, contributing to two-thirds of the greenhouse effect over the past decade. This study focuses on the chemical activation of avocado seeds with sodium hydroxide (NaOH). The influence of various preparation methods was studied under the same parameters: carbon precursor to NaOH mass ratio, carbonization temperature, and nitrogen flow. For two samples, preliminary thermal treatment was applied (500 °C). NaOH was used in the form of a saturated solution as well as dry NaOH. The same temperature of 850 °C of carbonization combined with chemical activation was applied for all samples. The applied modifications resulted in the following textural parameters: specific surface area from 696 to 1217 m<sup>2</sup>/g, total pore volume from 0.440 to 0.761 cm<sup>3</sup>/g, micropore volume from 0.159 to 0.418 cm<sup>3</sup>/g. The textural parameters were estimated based on nitrogen sorption at −196 °C. The XRD measurements and SEM pictures were also performed. CO<sub>2</sub> adsorption was performed at temperatures of 0, 10, 20, and 30 °C and pressure up to 1 bar. In order to calculate the CO<sub>2</sub> selectivity over N<sub>2</sub> nitrogen adsorption at 20 °C was investigated. The highest CO<sub>2</sub> adsorption (4.90 mmol/g) at 1 bar and 0 °C was achieved.

**Keywords:** sodium hydroxide; CO<sub>2</sub> adsorption; avocado seed; activated carbons



**Citation:** Siemak, J.; Mikołajczak, G.; Pol-Szyszko, M.; Michalkiewicz, B. Activated Carbon for CO<sub>2</sub> Adsorption from Avocado Seeds Activated with NaOH: The Significance of the Production Method. *Materials* **2024**, *17*, 4157. <https://doi.org/10.3390/ma17164157>

Academic Editors: Jerzy P. Lukaszewicz, Piotr Kamedulski and Maria Giorgia Cutrufello

Received: 14 July 2024

Revised: 19 August 2024

Accepted: 20 August 2024

Published: 22 August 2024



**Copyright:** © 2024 by the authors. Licensee MDPI, Basel, Switzerland. This article is an open access article distributed under the terms and conditions of the Creative Commons Attribution (CC BY) license (<https://creativecommons.org/licenses/by/4.0/>).

## 1. Introduction

The issue of global warming has been a worldwide priority for years, yet efforts to mitigate its effects remain insufficient. Recently, heightened attention to this issue has underscored that climate change, driven by greenhouse gas emissions, is raising alarm and making many people feel increasingly threatened [1,2]. Carbon dioxide is the most significant human-produced greenhouse gas, contributing to 77% of the anthropogenic greenhouse effect over the past decade, which translates to 26–30% of all CO<sub>2</sub> emissions [3]. The primary source of human-related CO<sub>2</sub> emissions is the burning of fossil fuels. The concentration of CO<sub>2</sub> in flue gases varies depending on the type of fuel used; for example, coal results in 12–15 mol % CO<sub>2</sub>. In industries such as petroleum refining and other manufacturing processes, the CO<sub>2</sub> levels in exhaust gases are process-dependent. For instance, oil refining emits 8–9 mol % CO<sub>2</sub>, cement production releases 14–33 mol % CO<sub>2</sub>, and iron and steel manufacturing results in 20–44 mol % CO<sub>2</sub> [4].

There are multiple approaches to decreasing atmospheric CO<sub>2</sub> emissions, such as the following: (a) improving the energy efficiency of fuels; (b) replacing fossil fuels with

renewable energy sources like wind, solar, biomass, and geothermal power; (c) transitioning to technologies that use low-carbon energy sources such as natural gas; (d) reducing overall energy consumption; and (e) implementing pre-combustion, post-combustion, and oxy-combustion CO<sub>2</sub> capture scenarios [5].

Additionally, more environmentally friendly and sustainable methods for CO<sub>2</sub> capture have been explored, including the use of porous materials, especially carbon-based materials [6–8]. Carbon-based materials are renowned for their exceptional properties, such as adjustable and modifiable functionality, high surface area and total pore volume, especially micropore volume, broad temperature range for CO<sub>2</sub> adsorption, rapid sorption kinetics, and excellent regeneration capabilities. In addition, these materials are cost-effective, industrially viable, and environmentally friendly [9,10]. They can be derived from a wide range of sources, and it is particularly worth highlighting that they can come from waste, especially from the food or agricultural industry [11,12].

Good CO<sub>2</sub> sorbents prepared from a carbon source require chemical activation. KOH is mainly applied as the activation agent. Sometimes H<sub>3</sub>PO<sub>4</sub>, K<sub>2</sub>CO<sub>3</sub>, ZnCl<sub>2</sub>, and CaCl<sub>2</sub> are also used to activate carbon production. NaOH is used very rarely in comparison to KOH. [11]. The reason is that usually activated carbons produced using NaOH showed much lower CO<sub>2</sub> adsorption than activated carbons produced using KOH [13].

Nurfarhana et al. [14] used NaOH to treat natural rubber, converting it into activated carbon for CO<sub>2</sub> adsorption. Natural rubber was carbonized at 400 °C for 2 h in a muffle furnace under a nitrogen flow. The pre-carbonized material was then mixed with solid NaOH at various ratios, ranging from 1:1 to 1:4 (natural rubber to NaOH). The activation process occurred in a tube furnace at 800 °C under a nitrogen atmosphere. Among all the samples, the highest specific surface area and total pore volume were achieved with a natural rubber to NaOH ratio of 1:4, reaching 1670 m<sup>2</sup>/g and 1.01 cm<sup>3</sup>/g, respectively. However, the CO<sub>2</sub> adsorption for the mass ratio of 1:1 was relatively low, with a value of 0.69 mmol/g at 25 °C and 1 bar pressure. In contrast, the CO<sub>2</sub> adsorption for the activated carbon obtained with a 1:4 ratio significantly increased to 2.98 mmol/g.

Dehkordi et al. [15] impregnated coal with NaOH solutions of varying concentrations (0.01–8 M) over different durations (4–7 h). Following impregnation, the coal samples were filtered and dried in an oven at 110 °C for 4–7 h. To examine the impact of washing on the activated carbon, some samples were immersed in deionized water. This study aimed to explore how different preparation parameters affect the surface properties and CO<sub>2</sub> adsorption capacity of the activated carbon. The ideal conditions for good CO<sub>2</sub> sorbent (51.4 mg/g) involved impregnation with a 1 M NaOH solution, followed by 6 h of mixing using a magnetic stirrer, without subsequent washing. The drying duration of the activated carbon had a minimal impact on its adsorption capacity.

Sodium hydroxide was used in the synthesis of sludge-activated carbon [16]. The carbon source was treated with a 5 wt % NaOH solution for 24 h. Following this, the reaction mixture was suction-filtered until the pH matched that of distilled water. Compared to the starting material, the specific surface area and pore volume of the sample treated with NaOH increased by 162% and 148%, respectively. The CO<sub>2</sub> adsorption at a pressure of 4 MPa reached 65 cm<sup>3</sup>/g.

Solid monolithic graphene oxides (MGOs) were also used in the production of porous carbon using NaOH [17]. Graphene oxide (GO) was transformed into MGOs through a self-assembled reduction process at 90 °C, employing various weight ratios of oxalic acid (1:1, 1:0.500, and 1:0.250). Following this, the monoliths underwent carbonization at 600 °C and were chemically activated using different NaOH ratios (1:1, 1:2, and 1:3).

Increasing the mass ratios of MGO to NaOH from 1:1 to 1:2 led to a surface area increase of approximately 2.6 times, ranging from 520.8 to 753.9 m<sup>2</sup>/g (the surface area of untreated MGO was 289.2 m<sup>2</sup>/g). As a result, this significantly boosted the CO<sub>2</sub> capture capacity to 2.10 mmol/g at a temperature of 25 °C and pressure of 1 bar.

Table 1 compares the activated carbon prepared using NaOH and standard materials (graphene and silica gel), focusing on the preparation method, properties, and CO<sub>2</sub> adsorption capacities, with published literature.

**Table 1.** The activated carbons prepared using NaOH.

Sorbent	Method of Preparation	SSA (m <sup>2</sup> /g) V <sub>tot</sub> (cm <sup>3</sup> /g)	q <sub>CO<sub>2</sub></sub> (mmol/g)	t (°C) p (bar)	Ref.
AC from natural rubber	carbonized at 400 °C; mixed with solid NaOH at ratios ranging from 1:1 to 1:4 (natural rubber to NaOH); activation at 800 °C	1670 m <sup>2</sup> /g 1.01 cm <sup>3</sup> /g	2.98	25 1	[14]
AC from coal	impregnation with NaOH solutions concentrations (0.01–8 M), durations (4–7 h).	614 m <sup>2</sup> /g	1.68	25 2.12	[15]
AC from sludge	treating with a 5 wt % NaOH solution for 24 h; washing with water until the pH was neutral.	101 m <sup>2</sup> /g 0.123 cm <sup>3</sup> /g	2.90	30 40	[16]
AC from monolithic graphene oxides	mixed with NaOH at ratios ranging from 1 to 3; carbonized at 600 °C; washing with water until the pH was neutral.	754 m <sup>2</sup> /g 1.97 cm <sup>3</sup> /g	2.10	25 1	[17]
AC from waste tea	impregnation with solution of NaOH (mass ratio 1:1); carbonized at 600 °C; washing with water until the pH was neutral.	270 m <sup>2</sup> /g 0.106 cm <sup>3</sup> /g	0.96	25 1	[18]
Graphene-hydrazine	graphite oxide was treated by hydrazine hydrate at a temperature of 90 °C	409 m <sup>2</sup> /g 0.48 cm <sup>3</sup> /g	1.44	0 1	[19]
SBA-15 modified by BTESE	TEOS was replaced by 10% of 3-(triethoxysilyl) propylamine.	269 m <sup>2</sup> /g 0.36 cm <sup>3</sup> /g	1.21	30 1	[20]

Nitrogen adsorption studies at −196 °C and carbon dioxide adsorption in the temperature range of 0–30 °C form the basis of our research. Therefore, we present the theoretical foundations about isotherms and hysteresis loops as outlined in the fundamental literature on this subject, recommended by IUPAC [21,22].

Physisorption isotherms can generally be categorized into six types [21]. Type I isotherms are characteristic of microporous solids and are concave to the p/p<sub>0</sub> axis, approaching a limiting value as p/p<sub>0</sub> approaches 1. Type II isotherms are typical of non-porous or macroporous adsorbents and are reversible. Type III isotherms are less common, convex to the p/p<sub>0</sub> axis throughout, and occur when adsorbate–adsorbate interactions are significant. Type IV isotherms are associated with mesoporous materials and feature a hysteresis loop due to capillary condensation within the mesopores and a limiting uptake at high p/p<sub>0</sub>. The initial section of a Type IV isotherm is indicative of monolayer–multilayer adsorption. Type V isotherms resemble Type III but include a hysteresis loop, observed in certain porous adsorbents with weak adsorbent–adsorbate interactions. Finally, Type VI isotherms represent stepwise multilayer adsorption on a uniform non-porous surface, with the sharpness of the steps varying depending on the system and temperature.

In the 1985 IUPAC recommendations, physisorption isotherms were categorized into six types. However, in 2015, Type I was further subdivided into Types Ia and Ib. Type Ia is characterized by a very steep uptake at very low p/p<sub>0</sub>, whereas for Type Ib, the uptake at very low p/p<sub>0</sub> is much milder. Type Ia isotherms are typical of microporous materials with predominantly narrow micropores (diameter smaller than 1 nm). In contrast, Type Ib isotherms are observed in materials with a broader pore size distribution, including wider micropores and possibly narrow mesopores (diameter smaller than 2.5 nm).

In the original 1985 IUPAC classification, four types of hysteresis loops were identified [21]. This classification was expanded to six types in 2015 [22]. The shape of hysteresis loops is closely linked to specific characteristics of the pore structure and the underlying adsorption mechanism.

In Type H1, the two branches are almost vertical and nearly parallel over a significant range of gas uptake. This loop is typically found in materials with a narrow range of uniform mesopores. Additionally, Type H1 hysteresis can appear in networks of ink-bottle pores where the neck size distribution is similar to the pore/cavity size distribution. Type H2(a) loops are characterized by a very steep desorption branch. This feature can be attributed to pore-blocking/percolation in a narrow range of pore necks or to cavitation-induced evaporation. Type H2(b) loops are also associated with pore blocking, but the neck size distribution is much broader. H2(a) loops are commonly found in silica gels, some porous glasses, and certain ordered mesoporous materials. The Type H3 loop resembles a Type II isotherm on the adsorption branch, and the lower limit of the desorption branch is usually at the cavitation-induced  $p/p_0$ . This loop occurs in non-rigid aggregates of plate-like particles and in pore networks with macropores that are not completely filled with pore condensate. Type H4 loops have nearly horizontal and parallel branches over a wide range of  $p/p_0$ . This loop is associated with the filling of micropores and is found in micro–mesoporous carbons. Type H5 loops are unusual and have a distinctive form associated with pore structures containing both open and partially blocked mesopores.

When using chemical activation, activated carbons are typically produced without temperature pretreatment. However, if temperature pretreatment is applied, authors do not compare these two methods. Similarly, the activating agent is commonly used in solution form, although the dry form is rarely used. No one has compared materials produced using the activating agent in both dry and dissolved forms until now.

The international market for avocado fruit and its derivatives (primarily guacamole and avocado oil) has been growing rapidly in the last decade [23]. Only the avocado pulp is employed for commercial applications, while other fruit elements like the seed and peel have no practical use and are disposed of by landfilling. Avocado seeds, which represent up to 26 wt % of the fruit mass, are produced in large amounts in centralized avocado transformation plants. Nevertheless, the use of this carbon source for producing activated carbon has been described in only a few publications. Therefore, we decided to use avocado seeds for producing carbon materials for CO<sub>2</sub> adsorption. Our team is the only one investigating the potential of such utilization of these activated carbons.

Our studies concerned five activated carbons obtained using the same temperature (850 °C) of activation combined with carbonization and an equal mass ratio of carbon source to activator (1:1). NaOH was utilized in two different forms: solid NaOH and its saturated solution. Activated carbons were produced with and without preliminary carbonization. We used the relatively uncommon activator NaOH. KOH is commonly used. The reason is that usually activated carbons produced using NaOH showed much lower CO<sub>2</sub> adsorption than activated carbons produced using KOH. We demonstrate here that CO<sub>2</sub> adsorption using NaOH can also be high if the appropriate method is applied. Avocado seeds were used as the carbon source. Avocado seeds as a carbon source have been described in only a few publications, and only our team has successfully produced activated carbons from avocado seeds for effective CO<sub>2</sub> adsorption. The novelty of the work lies in comparing the obtained materials using dry NaOH and a saturated solution as the activating agent, as well as highlighting the significance of preliminary carbonization. We demonstrated the significant importance of both the form of NaOH and the use of preliminary carbonization. These factors influence both the properties of activated carbons and their CO<sub>2</sub> adsorption capacity.

## 2. Materials and Methods

### 2.1. Materials and Reagents

We used the following chemicals for the synthesis of activated carbon from avocado seeds: NaOH (Chempur, Piekary Śląskie, Poland, pure p.a.) and 35–38% hydrochloric acid (Chempur, pure p.a.). The avocado seeds were dried at 60 °C for 24 h before undergoing pretreatment at 500 °C and chemical activation. After drying, the seeds were crushed and powdered using a Royal RCMZ-800 (Royal Catering expondo GmbH, Berlin,

Germany) multi grinder. The powdered avocado seeds were then used for the production of activated carbon.

## 2.2. Activated Carbon Synthesis

Five activated carbons were prepared from avocado seeds as described in Table 2 and shown in Figure 1.

**Table 2.** Procedures of sample preparation.

C500_NaOH	avocado seeds powder → furnace 500 °C → NaOH solution → furnace 850 °C
C500_NaOHdry	avocado seeds powder → furnace 500 °C → NaOH dry → furnace 850 °C
C_NaOH	avocado seeds powder +NaOH solution → furnace 850 °C
C_NaOHdry	avocado seeds powder +NaOH dry → furnace 850 °C
C_NaOHdry+H <sub>2</sub> O	avocado seeds powder +NaOH dry + few drops of H <sub>2</sub> O → furnace 850 °C

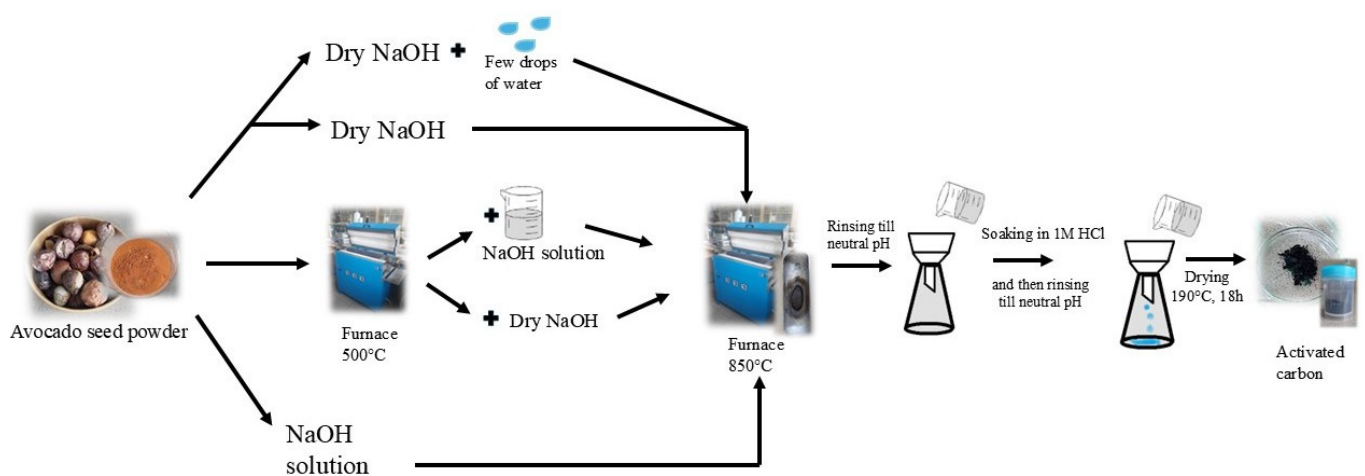


**Figure 1.** Activated carbon preparation from avocado seeds.

In the case of the first two samples, an initial pretreatment of avocado seed was conducted at 500 °C. Subsequently, samples were mixed with a saturated solution of NaOH (C500\_NaOH) or dry NaOH (C500\_NaOHdry), followed by carbonization at a temperature of 850 °C for 1 h under nitrogen flow. They were then washed with 1 M HCl and rinsed with distilled water until reaching neutral pH. The two other samples were obtained as described above but without preliminary thermal treatment. The dried, powdered avocado seeds were mixed with a saturated solution of NaOH (C\_NaOH) and dry NaOH (C\_NaOHdry). The sample C\_NaOHdry+H<sub>2</sub>O was obtained by mixing dried avocado seeds with dry NaOH and then adding some drops of water until the same pore volume of the starting materials was filled (incipient wetness method). In the incipient wetness method, only enough saturated NaOH solution is supplied to fill the pores of the starting materials. This minimizes the drying time of the sample, which reduces production costs. These costs are significantly lower than in the case of mixing the starting material with the saturated solution. In the latter method, the amount of saturated solution is such that the mass ratio of the carbon source to NaOH is 1. Here, we are dealing not only with the filling of the pores with the saturated solution.

## 2.3. Sample Characterization

The textural properties, including specific surface area (SSA), total pore volume ( $V_{\text{tot}}$ ), micropore volume ( $V_{\text{micro}}$ ), and pore size distribution in the range of 0.3 to 30 nm, were assessed using N<sub>2</sub> sorption at −196 °C. These measurements were conducted using an automatic volumetric adsorption device, the ASAP Sorption Surface Area and Pore Size Analyzer (ASAP 2460, Micrometrics, Novcross, GA, USA). The specific surface area was determined using the Brunauer–Emmett–Teller (BET) theory. The BET equation is useful

for determining the surface area of nonporous materials as well as those with macropores and mesopores (having sufficiently large pores) within the relative pressure range of  $p/p_0$  from 0.05 to 0.3. However, this method is not suitable for microporous adsorbents. Because the materials were mostly microporous, the method suggested by Rouquerol et al. [24] was applied. The procedure relies on two criteria: (a) the constant  $C$  must be positive, and (b) the use of the BET equation must be confined to the range where the term  $V(1-p/p_0)$  consistently increases with  $p/p_0$ . The relative range for surface area calculation was selected individually for each sample, also considering the value of the correlation coefficient, and ranged between  $5 \times 10^{-5}$  and  $1 \times 10^{-2}$  for microporous materials and ranged between  $1 \times 10^{-2}$  and  $2 \times 10^{-1}$   $C_{NaOHdry}$ .

The total pore volumes were determined from the volume of nitrogen adsorbed at a relative pressure close to  $p/p_0 \approx 1$ . The pore size distribution and micropore volumes were estimated using the density functional theory ( $N_2$ -DFT model for slit pores). Equilibrium adsorption isotherms of carbon dioxide at temperatures ranging from 0 to 30 °C and nitrogen at 20 °C were measured volumetrically using the ASAP Sorption Surface Area and Pore Size Analyzer (ASAP 2460, Micrometrics, Novcross, GA, USA), with pressures up to 1 bar. We select  $CO_2$  adsorption at a temperature range of 0–30 °C because this range is most popular in the investigations. We can easily compare our results with those of other researchers.

Phase analysis of the activated carbons was conducted using an X-ray diffractometer equipped with a Cu lamp by PANalytical Empyrean.

The average graphene sheet diameter ( $L_a$ ) and average crystallite thickness ( $L_c$ ) were approximately calculated using the Scherrer equation [25]. Liu et al. [26] suggested  $K = 1.84$  for the average graphene sheet diameter and  $K = 0.89$  for the average crystallite thickness. The number of graphitic layers ( $N$ ) was estimated using Equation (1):

$$N = \frac{L_c}{d_{002}} \quad (1)$$

The structural morphology of the activated carbons was examined using ultra-high-resolution field-emission scanning electron microscopy (UHR FE-SEM, Hitachi SU8020 Hitachi Ltd., Tokyo, Japan). The powdered sample was mounted on the SEM stub using double-sided carbon tape. Images were captured with a 20 kV accelerating voltage using a triple detector system.

### 3. Results and Discussion

#### 3.1. Materials Characterization

The pore structure of activated carbons produced from avocado seeds was thoroughly investigated using  $N_2$  adsorption–desorption isotherms at  $-196$  °C. As depicted in Figure 2, all adsorption isotherms exhibit a rapid  $N_2$  uptake at low pressure (relative pressure below 0.01), suggesting the presence of micropores in all the samples. The isotherms of samples pretreated at 500 °C and the sample prepared using NaOH solution show a sharp knee and a plateau after rapid uptake, indicating microporous materials. The isotherms of C500\_NaOH and C500\_NaOHdry correspond to a typical Type I isotherm according to the IUPAC classification [21], indicating that they are predominantly microporous. The very narrow hysteresis of H4 type is also present, indicating the presence of slit pores. For C\_NaOH, we observed a mixed isotherm of Types I and II. This indicates the presence of micropores as well as macropores. For C\_NaOH at higher relative pressure ( $>0.9$ ), a significant increase in  $N_2$  adsorption is visible, which is evidence of the presence of macropores. The combined isotherms Types IV and II were identified for NaOHdry+ $H_2O$ , C\_NaOHdry. Type IV is characteristic of mesoporous materials. The very rapid uptake (Type II) at higher relative pressure ( $>0.9$ ) indicates the presence of macropores. All the samples reveal hysteresis loops H4, which prove the presence of narrow slit-like pores. The hysteresis loop usually points to the presence of mesopores, but narrow hysteresis combined with a Type I isotherm indicates also microporosity.

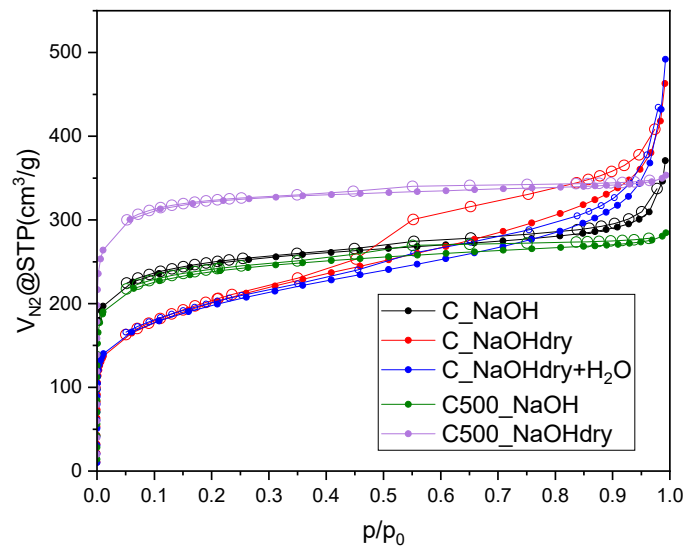


**Figure 2.** N<sub>2</sub> sorption isotherms measured at −196 °C, adsorption branch—filled symbols, desorption branch—empty symbols.

The results of the pore size distribution calculations performed using the DFT method, presented in Figure 3, and the values of the textural parameters in Table 3 confirm the conclusions drawn from the shapes of the N<sub>2</sub> adsorption isotherms. The pore size distribution curves (Figure 3) verify the microporous nature of C500\_NaOHdry, C500\_NaOH, and C\_NaOH. The most microporosity resulted in significantly narrower and smaller ultramicropores (>0.7 nm). was observed for C500\_NaOHdry. In contrast, C\_NaOHdry and C\_NaOHdry+H<sub>2</sub>O exhibited much wider and larger pores ranging from 2 to 4 nm.

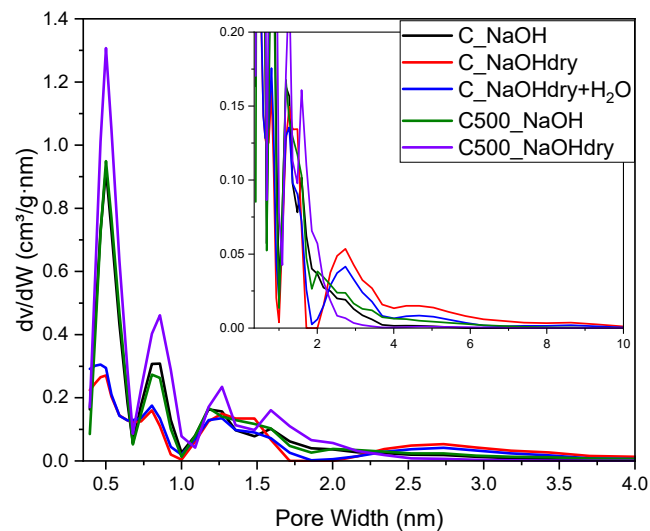


**Figure 3.** Pore size distribution of activated carbon.

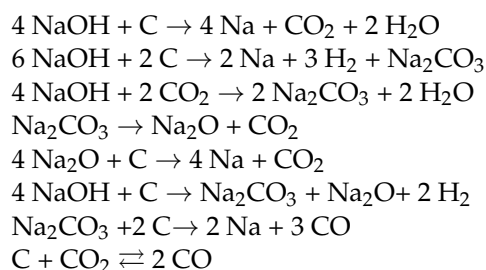
**Table 3.** Textural parameters of activated carbon.

AC	SSA (m <sup>2</sup> /g)	V <sub>tot</sub> (cm <sup>3</sup> /g)	V <sub>micro</sub> (cm <sup>3</sup> /g)	V <sub>micro/tot</sub> (%)
C_NaOH	918	0.574	0.295	51.39
C_NaOHdry	700	0.716	0.159	22.21
C_NaOHdry+H <sub>2</sub> O	696	0.761	0.168	22.08
C500_NaOH	885	0.440	0.290	65.91
C500_NaOHdry	1217	0.547	0.418	76.42

Based on Table 3, it can be discerned that the obtained specific surface areas range from 696 to 1217 m<sup>2</sup>/g, total pore volume ranges from 0.440 to 0.761 cm<sup>3</sup>/g, micropore volume ranges from 0.159 to 0.418 cm<sup>3</sup>/g, and the ratio of the two mentioned parameters ranges from 22.08% to 76.42%. Despite using the same carbonization temperature and quantity of activating agent, the samples obtained differed according to the preparation methods used. The highest  $V_{\text{micro}/\text{tot}}$  values are observed in the carbons that underwent preliminary thermal treatment of the seeds: C500\_NaOHdry (76.42%) and C500\_NaOH (65.91%).

It has been found that using a saturated NaOH solution as an activator for dry avocado seeds is more advantageous for developing porosity compared to using dry NaOH. The material activated with a saturated NaOH solution possessed a high specific surface area and micropore volume. The use of dry NaOH and dry avocado seeds was decidedly unfavorable. The situation was reversed when the activation was preceded by an initial pretreatment at a temperature of 500 °C. Activation of the resulting char with a saturated NaOH solution allowed for the production of a material with porosity comparable to that of C\_NaOH obtained without pretreatment. The textural parameters of C500\_NaOH were even lower. On the other hand, the activation of char after the pretreatment with dry NaOH enabled the production of a highly porous material with high micropore volume and specific surface area.

Based on theoretical considerations, the possible reaction between NaOH, carbon, and byproducts can be proposed as follows:

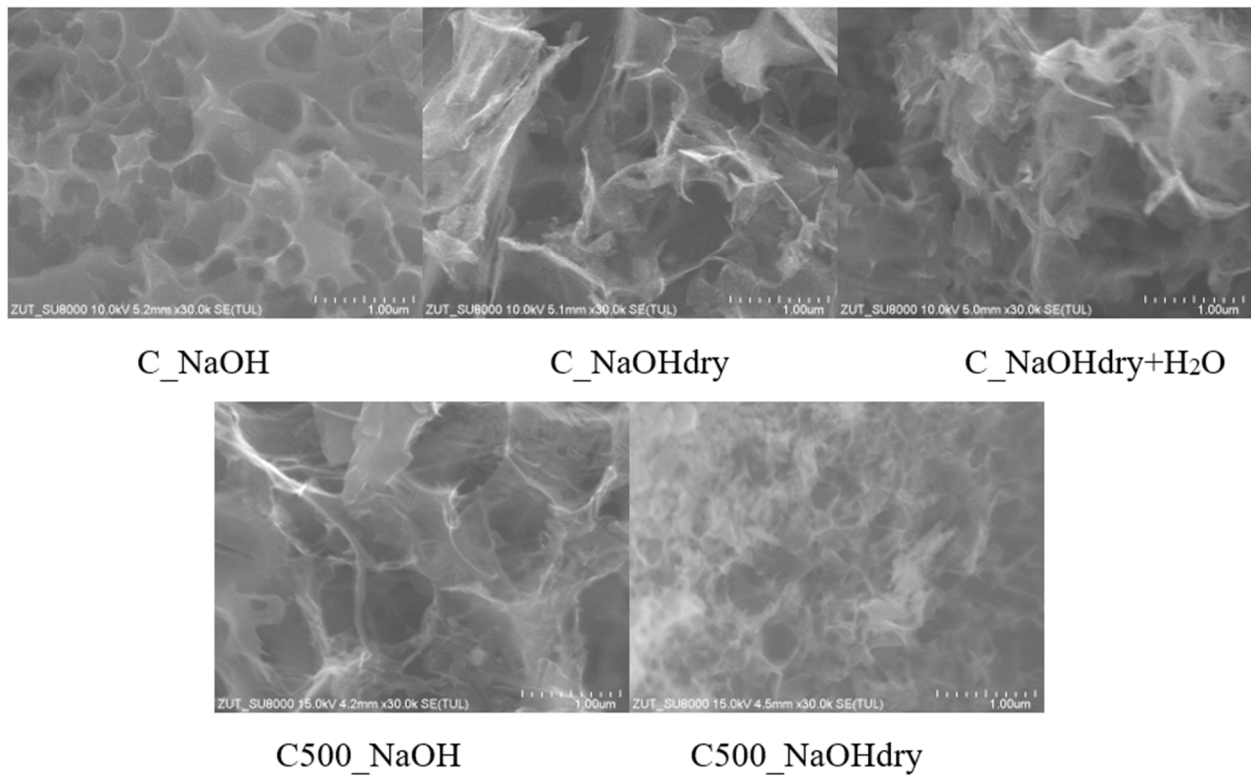


During the activation process, gases (H<sub>2</sub>, CO<sub>2</sub>, and CO), sodium, and sodium compounds (Na<sub>2</sub>O and Na<sub>2</sub>CO<sub>3</sub>). The reaction between the activating agent or byproducts and the carbon precursor leads to the breakdown of volatile organic compounds, resulting in the porous structure of the activated carbon samples. The gasification that occurs during activation with appropriate activating agents is crucial for the formation of pores. Thus, it can be argued that thermal treatment with an appropriate activating agent is essential for the formation of pores in activated carbon samples. During this process, the activating agent facilitates the development of a porous structure by promoting the removal of volatile substances and the creation of cavities. Without this step, the activated carbon would not exhibit the desired high surface area and porosity. Of course, both the choice of activating agent and the precise thermal conditions are crucial for producing high-quality activated carbon.

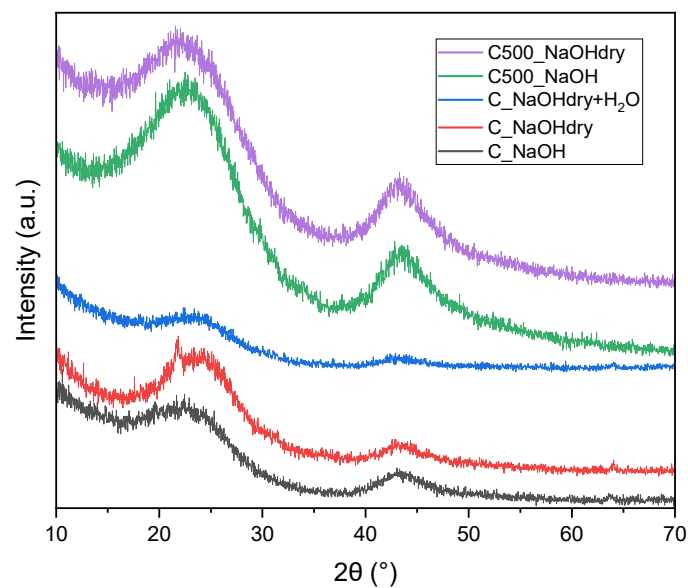
On the SEM images (Figure 4) of activated carbons with the highest specific surface area, such as C500\_NaOHdry and C\_NaOH, numerous macropores are observed, which, as commonly known, branch out into meso- and micropores within the material. For the material with the highest specific surface area (C500\_NaOHdry), macropores have significantly smaller diameters on the surface than those in C\_NaOH. In the case of other activated carbons with lower specific surface areas, the presence of thin, irregular planes creating occasional macropores with much larger sizes than in C\_NaOH was observed. SEM images confirm the results obtained based on nitrogen adsorption measurements at a temperature of −196 °C.

Figure 5 illustrates the XRD pattern of activated carbons activated by NaOH. Two broad peaks appearing around 22 and 44 degrees are observable. The shapes of these peaks suggest that the activated carbons derived from avocado seeds were predominantly amorphous.





**Figure 4.** SEM images (30,000× magnification).



**Figure 5.** XRD pattern of activated carbons.

The average crystallite thickness, number of graphitic layers, and average graphene sheet diameter calculated on the basis of XRD measurements are listed in Table 4. The average crystallite thickness of samples pretreated at 500 °C is the lowest, so the average number of layers in a stack is about 2. The average crystallite thickness of samples produced using dry NaOH without pretreatment is the highest. The average number of layers in a stack for these samples and for C\_NaOH are about 3. The average graphene sheet diameters of samples produced using dry NaOH without pretreatment are the highest, while C\_NaOH is the lowest. The results obtained from XRD studies are consistent with

the porosity analysis. The greatest disorder (the smallest average graphene sheet diameter) was observed for materials with the highest specific surface area.

**Table 4.** The average crystallite thickness ( $L_c$ ), number of graphitic layers ( $N$ ), and average graphene sheet diameter ( $L_a$ ).

AC	$L_c$ (nm)	$N$	$L_a$ (nm)
C_NaOH	1.04	2.71	2.39
C_NaOHdry	1.23	3.27	4.10
C_NaOHdry+H <sub>2</sub> O	1.23	3.30	3.69
C500_NaOH	0.88	2.29	3.45
C500_NaOHdry	1.04	2.71	2.39

CO<sub>2</sub> adsorption studies were conducted at four different temperatures: 0, 10, 20, and 30 °C and at a pressure of 1 bar. The results are presented in Table 5 and Figure 6.

**Table 5.** CO<sub>2</sub> and N<sub>2</sub> adsorption values over activated carbon.

AC	$q_{\text{CO}_2, 0\text{ }^\circ\text{C}}$ (mmol/g)	$q_{\text{CO}_2, 10\text{ }^\circ\text{C}}$ (mmol/g)	$q_{\text{CO}_2, 20\text{ }^\circ\text{C}}$ (mmol/g)	$q_{\text{CO}_2, 30\text{ }^\circ\text{C}}$ (mmol/g)	$q_{\text{N}_2, 20\text{ }^\circ\text{C}}$ (mmol/g)	$S_{\text{eq}}$
C_NaOH	3.69	3.07	2.57	2.12	0.38	6.76
C_NaOHdry	2.37	2.10	1.69	1.19	0.21	8.05
C_NaOHdry+H <sub>2</sub> O	2.56	2.16	1.64	1.21	0.21	7.81
C500_NaOH	4.20	3.50	2.96	2.46	0.37	8.00
C500_NaOHdry	4.90	4.00	3.37	2.76	0.50	6.84

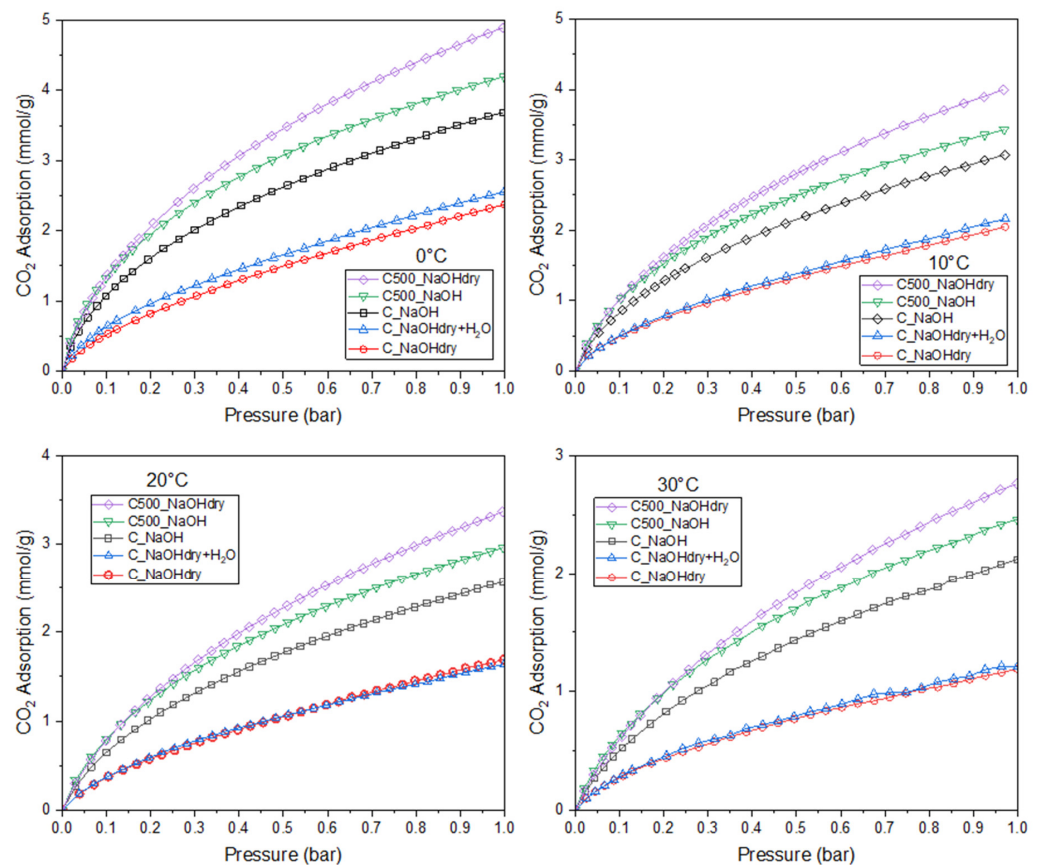


**Figure 6.** CO<sub>2</sub> adsorption isotherms at different temperatures.

Every sample exhibits a reduction in CO<sub>2</sub> adsorption with rising temperature, which is attributed to physisorption.

The CO<sub>2</sub> isotherms, measured up to 1 bar at temperatures of 0–30 °C, show that C500\_NaOHdry performs best at pressure below 1 bar. These observations can be rationalized by noting that C500\_NaOHdry has the largest volumes of micropores, which are effective in adsorbing CO<sub>2</sub> at pressure below 1 bar. The lowest CO<sub>2</sub> adsorption was observed in activated carbons with the smallest micropore volume (C\_NaOHdry and C\_NaOHdry+H<sub>2</sub>O). The relationship between CO<sub>2</sub> adsorption and micropore volume for all temperatures is presented in Figure 7. The micropore volume exhibited a very close correlation with CO<sub>2</sub> adsorption, having R<sup>2</sup> values higher than 0.9. This outcome aligns with findings from recent research studies [27,28].

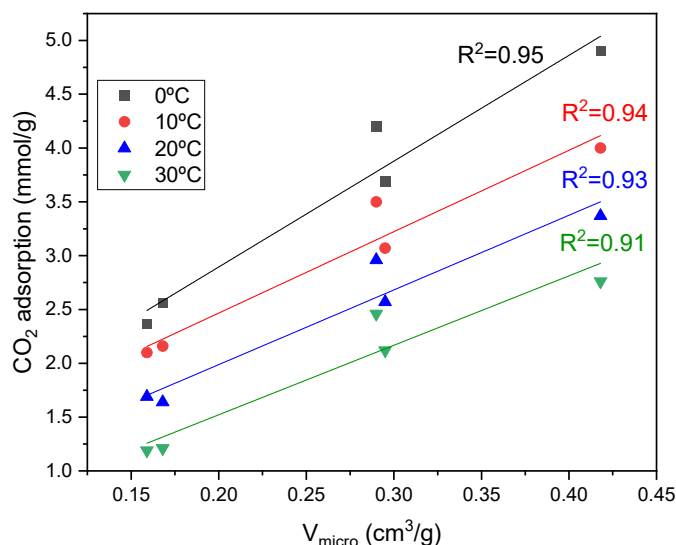


Figure 7. Correlation between CO<sub>2</sub> adsorption and micropore volume.

The CO<sub>2</sub> selectivity over N<sub>2</sub> nitrogen adsorption at a temperature of 20 °C was calculated. The adsorption of nitrogen at a temperature of 20 °C was very low compared to the adsorption of CO<sub>2</sub> at the same temperature (Figure 8).

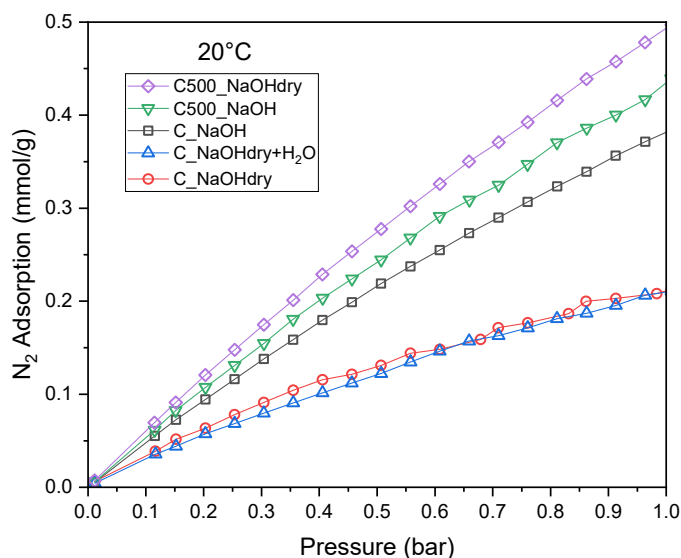


Figure 8. N<sub>2</sub> adsorption isotherms.

Furthermore, the Ideal Adsorption Solution Theory (Equation (2)) was employed to calculate the theoretical selectivity of CO<sub>2</sub> adsorption over N<sub>2</sub> at a pressure of 1 bar and an equimolar composition. This approach is widely utilized to forecast the adsorption of individual components within gas mixtures based on data from single gas adsorption experiments.

$$S_{IAST} = \frac{q_{CO_2}@p_{CO_2}/q_{N_2}@p_{N_2}}{p_{CO_2}/p_{N_2}} \quad (2)$$

where  $q_j @ p_i$  is the adsorption capacity of  $i$  at pressure  $p_i$ .

For equimolar composition, Equation (2) simplifies to Equation (3).

$$S_{CO_2/N_2} = \frac{q_{CO_2}(p)}{q_{N_2}(p)} \quad (3)$$

The results of selectivity of CO<sub>2</sub> adsorption over N<sub>2</sub> for equimolar composition ( $S_{eq}$ ) at 1 bar are presented in Table 5. The selectivity values are quite high and vary from 6.76 to 8.05.

Based on CO<sub>2</sub> and N<sub>2</sub> adsorption measurements, it is possible to determine the selectivity of CO<sub>2</sub> adsorption over N<sub>2</sub> using the IAST method across the entire pressure range. To achieve this, it is necessary to establish an adsorption model that best fits the experimental data. The adsorption model also allows for the calculation of the isosteric heat of CO<sub>2</sub> adsorption, which is extremely important.

The two-parameter (Langmuir [29] and Freundlich [30]) and three-parameter (Sips [31], Toth [32], and Radke–Prausnitz [33]) models were employed to fit the experimental data. To evaluate the appropriateness of fitting isotherm models to the experimental data, the Hybrid Error Function (HYBRID) [34] was utilized. The sum of squared errors (SSE) is commonly employed to measure the disparity between observed data and the true mean. To enhance SSE at lower pressure values, each square of the error values was divided by the experimental CO<sub>2</sub> adsorption value.

### 3.2. Studies on C500\_NaOHdry as Potential CO<sub>2</sub> Adsorbent

Among all the models, the Radke–Prausnitz model provided the highest accuracy in estimations for CO<sub>2</sub> adsorption, with the Hybrid Error Function not higher than 0.001. For N<sub>2</sub> adsorption, the best fit was ascertained for the Toth model with HYBRID equal to 0.00011. The constants of the Radke–Prausnitz and Toth models for the best adsorbent (C500\_NaOHdry) are collected in Table 6.

**Table 6.** The constants of Radke–Prausnitz and Toth models for C500\_NaOHdry.

	Radke–Prausnitz Model for CO <sub>2</sub>				Toth Model for N <sub>2</sub>	
	Temperature [°C]					
	0	10	20	30	20	
$q_{mRP}$	5.76	5.01	4.39	3.83	$q_{mT}$	3.01
$b_{RP}$	5.81	4.39	3.33	2.61	$b_T$	0.21
$n_{RP}$	0.59	0.59	0.59	0.6	$n_T$	0.90
HYBRID	0.00103	0.00078	0.00028	0.00081	HYBRID	0.00011

The Radke–Prausnitz equation is formulated as follows:

$$q = \frac{q_{mRP} \cdot b_{RP} \cdot p}{1 + b_{RP} \cdot p^{n_{RP}}} \text{ [mmol/g]} \quad (4)$$

$q_{mRP}$ —the maximum adsorption capacity [mmol/g];

$b_{RP}$ —the Radke–Prausnitz constant [ $\text{bar}^{-1}$ ];

$n_{RP}$ —Radke–Prausnitz model exponent.

Equation (5) outlines the Toth equation.

$$q = \frac{q_{mT} b_T p}{(1 + (b_T p)^{n_T})^{\frac{1}{n_T}}} [\text{mmol/g}] \quad (5)$$

$q_{mT}$ —the maximum adsorption capacity [mmol/g];

$b_T$ —the Toth constant [ $\text{bar}^{-1}$ ];

$n_T$ —the heterogeneity factor.

On the basis of the adsorption equilibrium models (2) and (3), the  $\text{CO}_2$  selectivity over  $\text{N}_2$  for equimolar composition at the pressure up to 1 bar for C500\_NaOHdry was calculated and presented in Figure 9. The equimolar selectivity ranges from 19.17 to 6.84.

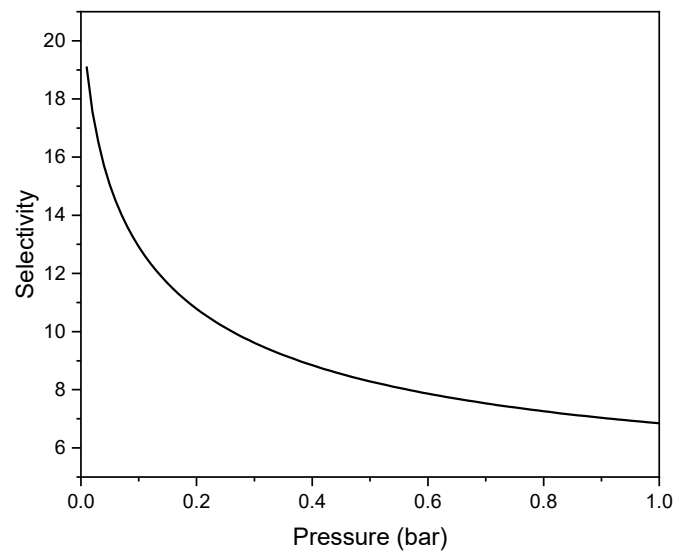


**Figure 9.** The  $\text{CO}_2$  selectivity over  $\text{N}_2$  for equimolar composition for the pressure up to 1 bar for C500\_NaOHdry.

Post-combustion capture involves extracting  $\text{CO}_2$  from flue gas after combustion. Typically, the  $\text{CO}_2$  in flue gas is mixed with inert gases like nitrogen, argon, water vapor, and oxygen, resulting in a dilution of around 8–15%  $\text{CO}_2$ . To determine if C500\_NaOHdry is suitable as an adsorbent for  $\text{CO}_2$  removal from flue gas after combustion using the IAST method, the  $\text{CO}_2$  adsorption selectivity over  $\text{N}_2$  was calculated for  $\text{CO}_2$  contents of 8% and 15%. The selectivity for  $\text{CO}_2$  removal from flue gas is 16.65 and 13.48, respectively, which indicates that C500\_NaOHdry is a potential sorbent for  $\text{CO}_2$  removal from flue gas.

The primary thermodynamic parameter of adsorption is the isosteric heat of adsorption. It can be determined from adsorption data at different temperatures by applying the Van't Hoff or Clausius–Clapeyron Equation (6).

$$Q_{iso} = -R \left( \frac{\partial \ln(p)}{\partial \left( \frac{1}{T} \right)} \right)_q \quad (6)$$

In order to apply Equation (6), the Radke–Prausnitz Equation (4) along with the parameters listed in Table 6 were used to compute the pressure values for the five specified surface coverage levels. Since it is not possible to solve Equation (4) algebraically for pressure, numerical methods were utilized instead. By plotting  $\ln(p)$  against the inverse of the absolute temperature ( $1/T$ ) for each loading, straight lines were produced, each having a slope of  $-Q_{iso}/R$ . This method enables the calculation of the isosteric heat of adsorption for the five specified surface coverage levels (Figure 10).

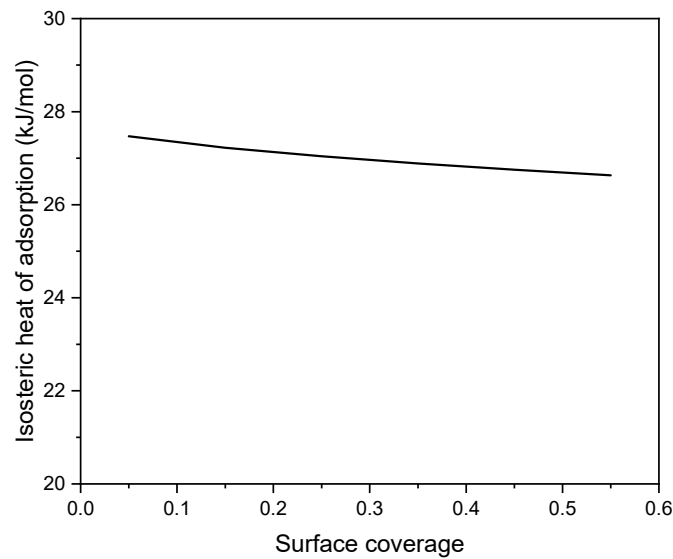


**Figure 10.** Isosteric heat of adsorption over C500\_NaOHdry versus surface coverage.

A high isosteric heat of adsorption generally indicates stronger interactions between the adsorbate and the adsorbent. The isosteric heat of adsorption values are below 50 kJ/mol, suggesting that CO<sub>2</sub> adsorption over C500\_NaOHdry samples is primarily of a physical nature. The isosteric heat of adsorption up to 0.5 surface coverage remains essentially constant, ranging from 27.4 to 26.6 kJ/mol. Such consistent values are highly favorable for CO<sub>2</sub> sorbent. CO<sub>2</sub> molecules are bound to the C500\_NaOHdry sorbent with moderate strength, allowing for desorption without excessive energy input. Materials with a higher isosteric heat of adsorption than C500\_NaOHdry will require more energy to desorb CO<sub>2</sub>, making the desorption process more costly. It is important to emphasize that the heat of adsorption on C500\_NaOHdry is extremely close to the heat of liquefaction of CO<sub>2</sub> (25 kJ/mol), which is the lower limit for the isosteric heat of adsorption. Therefore, this material ensures the lowest adsorption costs.

Figure 11 shows adsorption–desorption isotherms at temperatures of 10 and 30 °C for C500\_NaOHdry. The adsorption and desorption branches are nearly the same. The desorption isotherms lie slightly above the adsorption isotherms. Very narrow hysteresis is observed. The absorbed CO<sub>2</sub> was completely released at low pressures, confirming the very weak interaction between CO<sub>2</sub> and the sorbent [35].

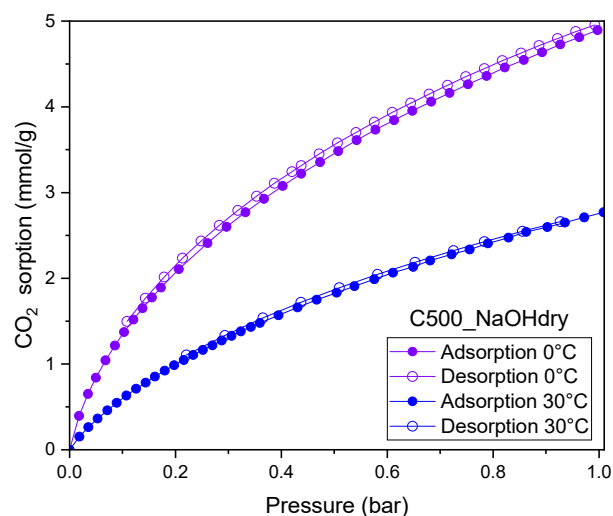


**Figure 11.** CO<sub>2</sub> sorption isotherms measured at 10 and 30 °C for C500\_NaOHdry.

#### 4. Conclusions

This study focuses on the chemical activation of avocado seeds with NaOH. The influence of various preparation methods has been studied under the same parameters: carbon precursor to NaOH mass ratio, carbonization temperature, and nitrogen flow. We demonstrate here that CO<sub>2</sub> adsorption using NaOH can be high if the appropriate method is applied.

The novelty of the work lies in comparing the obtained materials using dry NaOH and a saturated solution as the activating agent, as well as highlighting the significance of preliminary carbonization. We showed that preliminary carbonization at temperatures of 500 °C considerably improves CO<sub>2</sub> uptake.

The significant importance of both the form of NaOH and the use of preliminary carbonization as parameters were demonstrated. The highest values of textural parameters and CO<sub>2</sub> adsorption were achieved using thermal pretreatment and dry NaOH as the activating agent (C500\_NaOHdry). Activation with NaOH enlarged the pores, resulting in an impressive specific surface area (1217 m<sup>2</sup>/g) and a significant micropore volume (0.547 cm<sup>3</sup>/g). This facilitated CO<sub>2</sub> diffusion and adsorption (4.90 mmol CO<sub>2</sub>/g at 1 bar and 0 °C).

It was proven that the interaction between CO<sub>2</sub> and C500\_NaOHdry is very weak, and desorption is easy to achieve.

The equimolar CO<sub>2</sub> selectivity over N<sub>2</sub> was equal to 6.84, and for flue gas, it ranged from 16.65 to 13.48 depending on the CO<sub>2</sub> content. The adsorbent exhibited quite low isosteric heat of adsorption, about 27 kJ/mol. All the values of selectivity and isosteric heat of adsorption indicate that C500\_NaOHdry is a promising sorbent for CO<sub>2</sub> capture from flue gas.

Of the various isotherm equations, the Radke–Prausnitz model proved effective in accurately predicting CO<sub>2</sub> uptake isotherms.

In summary, the NaOH-activated carbon adsorbent exhibits potential for CO<sub>2</sub> adsorption and separation applications, demonstrating impressive CO<sub>2</sub> uptake and significant environmental benefits.

**Author Contributions:** Conceptualization, J.S. and B.M.; methodology, J.S. and B.M.; formal analysis, G.M.; investigation, J.S.; resources, M.P.-S.; writing—original draft preparation, J.S. and B.M.; writing—review and editing, J.S. and B.M.; visualization, J.S.; supervision, B.M. All authors have read and agreed to the published version of the manuscript.

**Funding:** This research received no external funding.

**Institutional Review Board Statement:** Not applicable.

**Informed Consent Statement:** Not applicable.

**Data Availability Statement:** The raw data supporting the conclusions of this article will be made available by the authors upon request.

**Conflicts of Interest:** The authors declare no conflicts of interest.

#### References

1. Li, S.; Yuan, X.; Deng, S.; Zhao, L.; Lee, K.B. A Review on Biomass-Derived CO<sub>2</sub> Adsorption Capture: Adsorbent, Adsorber, Adsorption, and Advice. *Renew. Sustain. Energy Rev.* **2021**, *152*, 111708. [[CrossRef](#)]
2. Song, C.; Liu, Q.; Ji, N.; Deng, S.; Zhao, J.; Li, Y.; Song, Y.; Li, H. Alternative Pathways for Efficient CO<sub>2</sub> Capture by Hybrid Processes—A Review. *Renew. Sustain. Energy Rev.* **2018**, *82*, 215–231. [[CrossRef](#)]
3. Vannak, H.; Osaka, Y.; Tsujiguchi, T.; Kodama, A. The Efficacy of Carbon Molecular Sieve and Solid Amine for CO<sub>2</sub> Separation from a Simulated Wet Flue Gas by an Internally Heated/Cooled Temperature Swing Adsorption Process. *Appl. Therm. Eng.* **2024**, *239*, 122145. [[CrossRef](#)]
4. Wei, R.; Alshahrani, T.; Chen, B.; Ibragimov, A.B.; Xu, H.; Gao, J. Advances in Porous Materials for Efficient Separation and Purification of Flue Gas. *Sep. Purif. Technol.* **2024**, *352*, 128238. [[CrossRef](#)]

5. Rahimi, V.; Ferreiro-Salgado, A.; Gómez-Díaz, D.; Sonia Freire, M.; González-Álvarez, J. Evaluating the Performance of Carbon-Based Adsorbents Fabricated from Renewable Biomass Precursors for Post-Combustion CO<sub>2</sub> Capture. *Sep. Purif. Technol.* **2024**, *344*, 127110. [[CrossRef](#)]
6. Tang, D.; Lyu, X.; Huang, Z.; Xu, R.; Chen, J.; Qiu, T. Nitrogen-Doped Microporous Carbons as Highly Efficient Adsorbents for CO<sub>2</sub> and Hg(II) Capture. *Powder Technol.* **2023**, *427*, 118769. [[CrossRef](#)]
7. Dindi, A.; Quang, D.V.; Vega, L.F.; Nashef, E.; Abu-Zahra, M.R.M. Applications of Fly Ash for CO<sub>2</sub> Capture, Utilization, and Storage. *J. CO<sub>2</sub> Util.* **2019**, *29*, 82–102. [[CrossRef](#)]
8. Xie, W.; Yao, X.; Li, H.; Li, H.; He, L. Biomass-Based N-Rich Porous Carbon Materials for CO<sub>2</sub> Capture and In-situ Conversion. *ChemSusChem* **2022**, *15*, e202201004. [[CrossRef](#)]
9. Sayari, A.; Belmabkhout, Y.; Serna-Guerrero, R. Flue Gas Treatment via CO<sub>2</sub> Adsorption. *Chem. Eng. J.* **2011**, *171*, 760–774. [[CrossRef](#)]
10. Sun, N.; Tang, Z.; Wei, W.; Snape, C.E.; Sun, Y. Solid Adsorbents for Low-Temperature CO<sub>2</sub> Capture with Low-Energy Penalties Leading to More Effective Integrated Solutions for Power Generation and Industrial Processes. *Front. Energy Res.* **2015**, *3*, 9. [[CrossRef](#)]
11. Ochedi, F.O.; Liu, Y.; Adewuyi, Y.G. State-of-the-Art Review on Capture of CO<sub>2</sub> Using Adsorbents Prepared from Waste Materials. *Process Saf. Environ. Prot.* **2020**, *139*, 1–25. [[CrossRef](#)]
12. Aghel, B.; Behaein, S.; Alobaid, F. CO<sub>2</sub> Capture from Biogas by Biomass-Based Adsorbents: A Review. *Fuel* **2022**, *328*, 125276. [[CrossRef](#)]
13. Kielbasa, K.; Bayar, Ş.; Varol, E.A.; Sreńscek-Nazzal, J.; Bosacka, M.; Miadlicki, P.; Serafin, J.; Wróbel, R.J.; Michalkiewicz, B. Carbon Dioxide Adsorption over Activated Carbons Produced from Molasses Using H<sub>2</sub>SO<sub>4</sub>, H<sub>3</sub>PO<sub>4</sub>, HCl, NaOH, and KOH as Activating Agents. *Molecules* **2022**, *27*, 7467. [[CrossRef](#)]
14. Nurfarhana, M.M.; Asikin-Mijan, N.; Yusoff, S.F.M. Porous Carbon from Natural Rubber for CO<sub>2</sub> Adsorption. *Mater. Chem. Phys.* **2023**, *308*, 128196. [[CrossRef](#)]
15. Dehkordi, S.S.R.; Delavar, Q.; Ebrahim, H.A.; Partash, S.S. CO<sub>2</sub> Adsorption by Coal-Based Activated Carbon Modified with Sodium Hydroxide. *Mater. Today Commun.* **2022**, *33*, 104776. [[CrossRef](#)]
16. Ma, J.; Liu, Y.; Chen, S.; Du, Y.; Wu, H. Changes in the Pore Structure of Modified Sludge-Activated Carbon and Its Effect on the Adsorption Characteristics of CO<sub>2</sub> under High Pressure. *Microporous Mesoporous Mater.* **2022**, *345*, 112255. [[CrossRef](#)]
17. Jha, R.K.; Bhunia, H.; Basu, S. Experimental Kinetics and Thermodynamics Investigation: Chemically Activated Carbon-Enriched Monolithic Reduced Graphene Oxide for Efficient CO<sub>2</sub> Capture. *Heliyon* **2024**, *10*, e27439. [[CrossRef](#)]
18. Tahmasebpour, M.; Iranvandi, M.; Heidari, M.; Azimi, B.; Pevida, C. Development of Novel Waste Tea-Derived Activated Carbon Promoted with SiO<sub>2</sub> Nanoparticles as Highly Robust and Easily Fluidizable Sorbent for Low-Temperature CO<sub>2</sub> Capture. *J. Environ. Chem. Eng.* **2023**, *11*, 110437. [[CrossRef](#)]
19. Singh, S.B.; De, M. Carbon Dioxide Removal by Chemically and Thermally Reduced Graphene-Based Adsorbents. *Korean J. Chem. Eng.* **2024**, *41*, 783–796. [[CrossRef](#)]
20. Avellaneda, G.L.; Denoyel, R.; Beurroies, I. CO<sub>2</sub>/H<sub>2</sub>O Adsorption and Co-Adsorption on Functionalized and Modified Mesoporous Silicas. *Microporous Mesoporous Mater.* **2024**, *363*, 112801. [[CrossRef](#)]
21. Sing, K.S.W. Reporting Physisorption Data for Gas/Solid Systems with Special Reference to the Determination of Surface Area and Porosity (Recommendations 1984). *Pure Appl. Chem.* **1985**, *57*, 603–619. [[CrossRef](#)]
22. Thommes, M.; Kaneko, K.; Neimark, A.V.; Olivier, J.P.; Rodriguez-Reinoso, F.; Rouquerol, J.; Sing, K.S.W. Physisorption of Gases, with Special Reference to the Evaluation of Surface Area and Pore Size Distribution (IUPAC Technical Report). *Pure Appl. Chem.* **2015**, *87*, 1051–1069. [[CrossRef](#)]
23. Domínguez, M.P.; Araus, K.; Bonert, P.; Sánchez, F.; San Miguel, G.; Toledo, M. The Avocado and Its Waste: An Approach of Fuel Potential/Application. In *Environment, Energy and Climate Change II*; Springer: Cham, Switzerland, 2014; pp. 199–223.
24. Rouquerol, J.; Llewellyn, P.; Rouquerol, F. Is the BET Equation Applicable to Microporous Adsorbents? *Stud. Surf. Sci. Catal.* **2007**, *160*, 49–56.
25. Cullity, B.D.; Weymouth, J.W. Elements of X-ray Diffraction. *Am. J. Phys.* **1957**, *25*, 394–395. [[CrossRef](#)]
26. Lu, L.; Sahajwalla, V.; Kong, C.; Harris, D. Quantitative X-ray Diffraction Analysis and Its Application to Various Coals. *Carbon* **2001**, *39*, 1821–1833. [[CrossRef](#)]
27. Singh, G.; Tiburcius, S.; Ruban, S.M.; Shanbhag, D.; Sathish, C.I.; Ramadass, K.; Vinu, A. Pure and Strontium Carbonate Nanoparticles Functionalized Microporous Carbons with High Specific Surface Areas Derived from Chitosan for CO<sub>2</sub> Adsorption. *Emergent Mater.* **2019**, *2*, 337–349. [[CrossRef](#)]
28. Serafin, J.; Sreńscek-Nazzal, J.; Kamińska, A.; Paszkiewicz, O.; Michalkiewicz, B. Management of Surgical Mask Waste to Activated Carbons for CO<sub>2</sub> Capture. *J. CO<sub>2</sub> Util.* **2022**, *59*, 101970. [[CrossRef](#)]
29. Elmorsi, T.M. Equilibrium Isotherms and Kinetic Studies of Removal of Methylene Blue Dye by Adsorption onto Miswak Leaves as a Natural Adsorbent. *J. Environ. Prot.* **2011**, *2*, 817–827. [[CrossRef](#)]
30. Travis, C.C.; Etnier, E.L. A Survey of Sorption Relationships for Reactive Solutes in Soil. *J. Environ. Qual.* **1981**, *10*, 8–17. [[CrossRef](#)]
31. Ayawei, N.; Angaye, S.S.; Wankasi, D.; Dikio, E.D. Synthesis, Characterization and Application of Mg/Al Layered Double Hydroxide for the Degradation of Congo Red in Aqueous Solution. *Open J. Phys. Chem.* **2015**, *5*, 56–70. [[CrossRef](#)]



32. Podder, M.S.; Majumder, C.B. Studies on the Removal of As(III) and As(V) through Their Adsorption onto Granular Activated Carbon/MnFe<sub>2</sub>O<sub>4</sub> Composite: Isotherm Studies and Error Analysis. *Compos. Interfaces* **2016**, *23*, 327–372. [[CrossRef](#)]
33. Tran, H.N.; Bollinger, J.-C.; Lima, E.C.; Juang, R.-S. How to Avoid Mistakes in Treating Adsorption Isotherm Data (Liquid and Solid Phases): Some Comments about Correctly Using Radke-Prausnitz Nonlinear Model and Langmuir Equilibrium Constant. *J. Environ. Manag.* **2023**, *325*, 116475. [[CrossRef](#)]
34. Kumar, K.V.; Porkodi, K.; Rocha, F. Comparison of Various Error Functions in Predicting the Optimum Isotherm by Linear and Non-Linear Regression Analysis for the Sorption of Basic Red 9 by Activated Carbon. *J. Hazard. Mater.* **2008**, *150*, 158–165. [[CrossRef](#)] [[PubMed](#)]
35. Sapchenko, S.A.; Barsukova, M.O.; Belosludov, R.V.; Kovalenko, K.A.; Samsonenko, D.G.; Poryvaev, A.S.; Sheveleva, A.M.; Fedin, M.V.; Bogomyakov, A.S.; Dybtsev, D.N.; et al. Understanding Hysteresis in Carbon Dioxide Sorption in Porous Metal–Organic Frameworks. *Inorg. Chem.* **2019**, *58*, 6811–6820. [[CrossRef](#)] [[PubMed](#)]

**Disclaimer/Publisher’s Note:** The statements, opinions and data contained in all publications are solely those of the individual author(s) and contributor(s) and not of MDPI and/or the editor(s). MDPI and/or the editor(s) disclaim responsibility for any injury to people or property resulting from any ideas, methods, instructions or products referred to in the content.